Nested Auto-Regressive Processes for MPEG-Encoded Video Traffic Modeling

Derong Liu, *Senior Member, IEEE*, Endre I. Sára, *Student Member, IEEE*, and Wei Sun, *Student Member, IEEE*

***Abstract*—This paper presents a new traffic model for MPEG-encoded video sequences. The hybrid Gamma/Pareto distribution is used for all three types of frames in MPEG-encoded video sequences, and the present model takes scene changes into account. The autocorrelation structure is modeled using two second-order auto-regressive (AR) processes nested with each other. One AR process is used to generate the mean frame size of the scenes to model the long-range dependence, and another AR process is used to generate the fluctuations within the scenes to model the short range dependence. The parameters of the AR processes are estimated from measurements of empirical video sequences. Simulation results show that the present model captures the autocorrelation structure in the empirical traces at both small and large lags. The MPEG traffic model presented in this paper is used to predict the queueing performance of single and multiplexed MPEG video sequences at an asynchronous transfer mode multiplexer. Comparison study shows that the present model provides accurate prediction for quality of service measures, such as cell-loss ratio under different traffic loads and various buffer sizes.**

***Index Terms*—Auto-regressive process, MPEG encoded video, traffic modeling, video modeling.**

I. Introduction

Multimedia applications such as video teleconferencing, video phone, and video-on-demand have been predicted to be the major sources of traffic for the Broadband Integrated Services Digital Networks (B-ISDN). Due to the extremely high bandwidth requirements of uncompressed video streams, many coding algorithms have been developed for video compression. The MPEG standards for video coding have gained world-wide acceptance and they are expected to play a dominant role in the foreseeable future. The MPEG coding utilizes both the spatial and the temporal redundancy of the video stream [12], [35], and [36]. Three frame types can be used within an MPEG video sequence. An I frame is an intra-coded frame (JPEG-like frame). A P frame is encoded with forward motion prediction, where macro-blocks are temporarily predicted from a previous I or P frame. A B frame is encoded with forward and/or backward predictions. A group of pictures (GOP) is a predefined pattern of I, P, and B frames, which defines the sequence of frame types in MPEG videos. For example, a GOP with 12 frames can be described by $IBBPBBPBBPBB$. In principle, however, the MPEG standards allow arbitrary length for GOPs and flexible arrangements of frame types in a GOP. The present study will be focused on fixed-size GOPs with deterministic, regular GOP patterns. Using MPEG standards, the *size* of video frames will vary drastically as the sequence is being generated/transmitted, and thus results in variable-bit-rate (VBR) traffic. In the present paper, we use the term "size" and "frame size" interchangeably to represent the number of data units (e.g., bits or cells) for each encoded video frame.

The technology selected to deliver the B-ISDN services is the asynchronous transfer mode (ATM) [28]; it transfers information through the network in fixed-size packets called cells. ATM allows the network to take advantage of the bit-rate variations of individual sources through statistical multiplexing. Video traffic models are needed for studying the performance of B-ISDN/ATM networks, either by means of analysis or simulation. The knowledge of the characteristics of traffic flowing in the network plays one of the most important roles in network design; accurate characterization of traffic streams is essential to dimensioning network resources and providing acceptable level of quality of service. The present study will concentrate on modeling the frame sizes of MPEG-encoded video sequences and on the queueing performance at an ATM multiplexer when video frame sequences are transmitted through an ATM network.

Video traffic modeling has been studied extensively and many results have been reported (for an overview, see, e.g., [1], [8], and [24]). The modeling approach for VBR video traffic can roughly be divided into several main classes, i.e., *histogram-based models* (e.g., [31], [32]), *Markov chain models* (e.g., [13], [14], [17], [22], [27], and [29]), *AR processes* (e.g., [5], [11], [16], [19], [20], [22], [25], [30], [33], and [34]), *self-similar or fractal models* (e.g., [2], [9], and [15]), and other approaches such as [4], [5], [7], [18], and [23]. Of particular interests in video traffic modeling are the frame-size distribution and the traffic correlation (autocorrelation between the frame sizes). The frame-size distribution has been studied in many existing works; the distributions studied include Normal distribution [25], Log normal distribution [19], Gamma distribution [14], and hybrid Gamma/Pareto distribution [9], [18]. On the other hand, modeling the traffic autocorrelation function is still an active research area. Most of the existing results can model the autocorrelation function at small lags [short-range dependence (SRD)] accurately, but many of them fail at modeling the autocorrelation function at large

Manuscript received June 7, 1999; revised June 1, 2000. This work was supported in part by the National Science Foundation under Grant ECS-9996428 and by Blonder Broadcasting Corporation, Morganville, NJ. This paper was recommended by Associate Editor H.-J. Zhang.

D. Liu is with the Department of Electrical Engineering and Computer Science, University of Illinois, Chicago, IL 60607 USA (e-mail: dliu@ieee.org).

E. I. Sára and W. Sun are with the Department of Electrical and Computer Engineering, Stevens Institute of Technology, Hoboken, NJ 07030 USA.

Publisher Item Identifier S 1051-8215(01)01242-3.

lags (long range dependence or LRD). Video traffic models can be classified according to the autocorrelation function as SRD and LRD models. The distinctive feature between SRD and LRD models [2] is whether the autocorrelation function $\rho(k)$ is summable, where $k = 1, 2, \ldots$ represents the frame lags. In particular, SRD models will have a rapid decay in the autocorrelation function at large lags resulting in a summable $\rho(k)$, i.e., $\sum_{k=1}^{\infty} \rho(k) < \infty$; while the autocorrelation function of LRD models drops off slowly to the extent that $\rho(k)$ is not summable, i.e., $\sum_{k=1}^{\infty} \rho(k) = \infty$. Several researchers have attempted to resolve the modeling of the autocorrelation function at large lags in video traffic. In [20], a linear combination of two first-order AR processes is used; one AR process contributes to the modeling of the autocorrelation function at small lags and the other to the modeling of the autocorrelation function at large lags. Improvements are achieved over the use of a single AR process for the modeling of the autocorrelation function in video traffic streams. The result in [20] is further modified in [30] by using a three-state Markov chain to characterize the scene changes in the linear combination of 2 first-order AR processes. Self-similar or fractal models have also been used to model the LRD (cf., [2], [9], and [15]).

In [18], $M/G/\infty$ input processes are used for video traffic modeling which the authors claim to have achieved a compromise between Markovian (SRD) and LRD models, though it is actually shown in [18] that the $M/G/\infty$ input processes result in SRD models. The resulting autocorrelation function has the form of $e^{-\beta\sqrt{k}}$, where $\beta > 0$ and k is the index of lags. It is argued in [18] that pure LRD models will inevitably miss the fitting of autocorrelation function at small lags.

In the present paper, a modeling approach is developed for frame-size sequences of MPEG videos based on *nested AR processes*. It is well known that AR processes can model the SRD but fail at modeling the LRD. In the present approach, a second-order AR process is used to model the SRD. By using another second-order AR process nested with the first AR process, we demonstrate in the present paper that the autocorrelation function at both small and large lags can be modeled accurately. We will also derive the analytical form of the autocorrelation function of the present model. One related existing work is [19] where MPEG video frame-size sequences are modeled as the superposition of an AR process (for SRD) with a sequence of i.i.d. random variables. The present approach replaces the i.i.d. random variables in the model of [19] with an AR process nested with the first AR process to provide a better match for the autocorrelation function at large lags. Another related existing work is [27], where nested Markov chains are used in the modeling of GOP size sequences for MPEG video traffic. The present approach is distinctive from that of [27] in the following two aspects: 1) the present approach models video traffic at the frame-size level while [27] models video traffic at the GOP size level and 2) the use of AR processes in the present approach are in general simpler in representation and easier in computation than the use of Markov chains. Although the model of [27] fits well the autocorrelation function of the empirical traces at the GOP level, it usually coarsens the time scale for more than 10 folds (from 30 to 40 ms to half seconds). We note that coarsening the time scale may not be desirable in the study of traffic for high-speed networks [5].

We will conduct simulation studies for a wide range of VBR streams including MPEG-2, MPEG-1, JPEG, and DCT video traces, where frame-size distributions and autocorrelation structures will be studied for each trace. Our simulation results will show a very good match for the autocorrelation function at both small and large lags. In addition, we will study the queueing performance (cell-loss ratio) of the present model using a single server with first-in–first-out (FIFO) queue to compare with the queueing performance of the empirical traces. Queueing performance and autocorrelation structures, together with the frame-size distributions, are some of the most important aspects in validating the appropriateness/accuracy of traffic models. In the present paper, we will investigate queueing performance for both single trace and multiplexed traces.

II. AR Processes and Traffic Scenes

In this section, we introduce the AR processes which are related to the present modeling effort. Consider a linear system with input $\{s(t)\}$ and output $\{y(t)\}$, where t is the discrete time. The finite AR processes are defined by (cf., [26])

$$y(t) = \sum_{k=1}^{p} a_k y(t-k) + s(t)$$

where $\{s(t)\}$ is an uncorrelated process with zero mean and variance σ^2, and $\{a_k, 1 \leq k \leq p\}$ is a finite sequence with $a_p \neq 0$. Such a process is denoted by AR(p) and p is called the order of the AR process. It is well known that when $\{s(t)\}$ is Normal, $\{y(t)\}$ will also be Normal.

There are a number of methods to estimate the parameters for an AR process given $\{y(t)\}$. These include the Yule–Walker estimation, Levinson–Durbin algorithm, maximum-entropy estimation, least-square estimation, maximum-likelihood estimation, and the like [26]. Least-square estimation will be used in the present study.

It has been observed and pointed out by several authors that the frame-size sequence of compressed videos shows scene changes [7], [13], [17], [19], and [21]. In a typical frame-size sequence (e.g., the I frame-size sequence of MPEG encoded video or the frame-size sequence of JPEG/DCT encoded video), there are periods where the frame-size changes are relatively small, and these periods are separated by large changes in the frame size. This is due to the scene changes in the video frame-size sequence. In our definition of scenes, each scene corresponds to a period where the frame-size changes are relatively small, and between two consecutive scenes, there is a large change in the frame size. It is important to note that the scenes in the frame-size sequence may not match with the scenes that the audience perceives. In a movie, for example, there may be a change in the picture, where the movie shows a completely different scene, but the frame size stays very close. In this case, we will not observe any scene changes in the frame-size sequence since the frames are all very close in size, even though the audience perceives a scene change since the movie has changed from one scene to another. Movies tend to have quick changes in the picture, where a considerable change in the frame size occurs every 2–5 min on average, or even more often. Document series or interviews may have longer scenes, but there will still be scene changes when switched to a new camera view or a new part of the program.

In the new traffic model developed in the present paper, scene changes will be incorporated into the modeling process and later into the generation of synthetic frame-size sequences. It is pointed out in [19] that incorporating a "scenic" component in a traffic model gives the VBR dynamics a physical interpretation and often leads to better performance predictions. The approach of [13] will be used to detect the scene changes where the second difference between frame sizes is obtained. The second difference is divided by the average frame size of a block of previous frames (e.g., 25 frames). If the result is large in magnitude and negative in sign, then we say that a scene change is detected. In other words, if

$$\frac{[X_I(n+1)-X_I(n)]-[X_I(n)-X_I(n-1)]}{(1/25)\sum_{j=n-24}^{n} X_I(j)} < -\lambda$$

a new scene is detected, where $X_I(n)$ is the nth I frame size of an MPEG video (or the nth frame size of a JPEG/DCT video) and $\lambda > 0$ is the threshold of burstiness. The length of each scene and the average frame size of each scene will be recorded. We will use these information later on for generating the frame-size sequences.

The scene-length distribution has been studied by several authors. In [7], a distribution similar to Cauchy distribution is proposed for the scene-length distribution. In [13], Gamma, Weibull, and the generalized Pareto distributions are used to model the scene-length distribution. In [19] and [21], geometric distribution is fitted for the scene-length distribution.

III. A New Traffic Model for MPEG-Encoded Video Sequences

A. Frame-Size Distributions

In the present study, we will use MPEG-2 encoded video sequences of the movie Titanic (more than three hours); these sequences will be broken down into three separate parts containing only the frame sizes of the I, P, or B type. This is because of the difficulty in modeling the complete video sequence with I, P, and B frames [19]. Separate models will be developed for the I, P, and B frame types. Several probability distribution functions are examined to fit the MPEG-2 empirical streams. For each frame type, Normal, Gamma, Log normal, and Pareto distributions are tried to fit the frame-size distribution.

Normal, Gamma, and Log normal distributions generally have bell-shaped density functions, and they all fit the main body of the empirical frame-size distribution well. Since the tail behavior (especially the right tail behavior) plays a very important role in determining the buffer overflow probability at a multiplexer [10], it will be investigated in fitting the empirical traces for probability distributions. Fig. 1 shows the right tail behavior of the I frame-size sequence of the movie Titanic (with GOP =15, i.e., $IBBPBBPBBPBBPBB$) using the log–log plot of the complimentary cumulative distribution function. It can be seen that a hybrid Gamma/Pareto distribution fits better than all the others. Figs. 2 and 3 show the results of the P and B frame-size sequences, respectively. The choice for the probability distribution of each frame type is determined from Figs. 1–3. We will use the hybrid Gamma/Pareto distribution for all three types of frame-size sequences. The hybrid Gamma/Pareto distribution was also used previously in the study in [9] and [18]. As in [9] and [18], the Gamma distribution is used to capture the general shape of

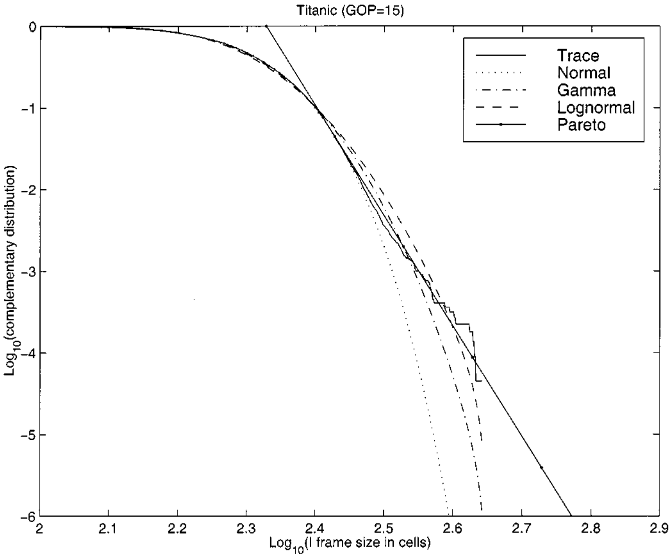

Fig. 1. I frame-size distribution.

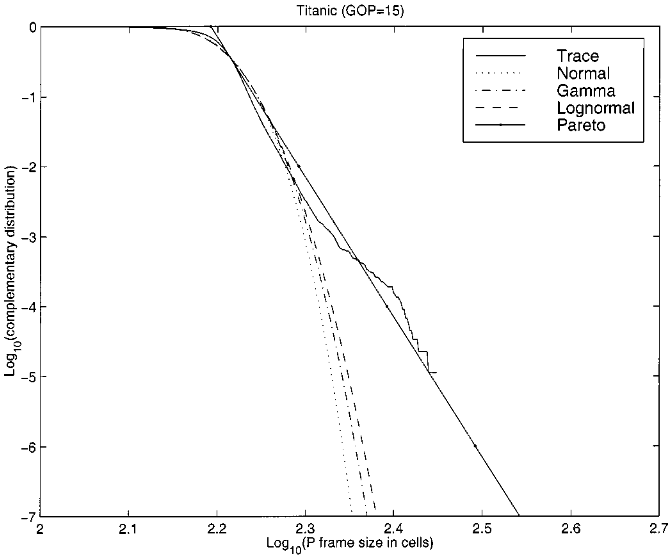

Fig. 2. P frame-size distribution.

the empirical distribution, and the Pareto distribution is used to capture the tail of the empirical distribution.

B. Nested AR Processes for Video Traffic Modeling

It has been pointed out in [19] that the effects of the correlations of the empirical P (also B) frame-size sequences are negligible compared to that of the empirical I frame-size sequence. Therefore, the P and B frame types will be modeled similarly as in [19] by two processes of i.i.d. random variables with estimated parameters. In the present study, we will incorporate scene changes in the modeling of the I frame sequence as described in Section II and we will ignore the scene changes in the P and B frame sequences [19]. If a single probability density function is used for the generation of I frames, the variation of the traffic will usually be higher than the variation of the empirical traffic within scenes (cf., [7], [13], [17], [19], and [21]).

Let $X_I(n)$ be the size (i.e., the number of bits or cells) of the nth I frame in an MPEG video sequence. $X_I(n)$ will be modeled as the sum of two independent random variables

$$X_I(n) = M_I(n) + \delta_I(n) \qquad (1)$$

where $M_I(n)$ is the mean frame size of the scene to which the nth I frame belongs and $\delta_I(n)$ represents the fluctuation of the nth I frame about the mean of the scene. For the jth scene with length N_j that starts at the kth I frame, $M_I(n)$ will take the same value for every frame within the scene, which will be denoted by another random variable $\tilde{X}_I(j)$, i.e.,

$$M_I(k) = M_I(k+1) = \ldots = M_I(k+N_j-1) \triangleq \tilde{X}_I(j).$$

The second random variable $\delta_I(n)$ in (1) is used to fit the sequence obtained from the original data by subtracting the mean of the scene [i.e., $M_I(n)$] from each frame within the scene. This process actually eliminates the scenes. As a result, $\delta_I(n)$ has zero mean and it models a "sceneless" sequence with a variance σ_δ^2 very close, or equal to, the variance of the video traffic within scenes.

Remark 3.1: With the random variables defined in the preceding, it is easily seen that $\{X_I(n)\}$, $\{M_I(n)\}$, $\{\delta_I(n)\}$, and $\{\tilde{X}_I(j)\}$ constitute stochastic processes. Stationarity will be assumed for *all* the processes used in the present paper. This is an assumption often used in video traffic modeling literature. It is also emphasized that $\{M_I(n)\}$ and $\{\delta_I(n)\}$ are assumed to be mutually independent in the present paper. ■

High correlation has been observed consistently in video frame-size sequences and it is due to similarities between frame sizes in the sequence. Data generated by video encoders are highly correlated due to the existence of similar sizes between distant frames, especially between distant I frames, regardless of the contents of the frames. Even though the content of the frames changes over time, distant frames may still have similar sizes. In the present modeling approach, the correlation is introduced through AR processes, which are used in generating the two independent variables in (1). In both cases, we employ the second-order AR process.

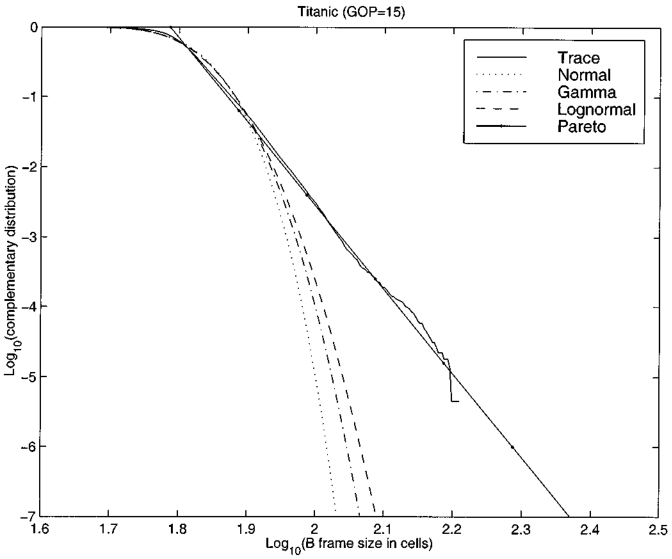

Fig. 3. B frame-size distribution.

To model the short range dependence, a second-order AR process is used for the sceneless sequence $\{\delta_I(n)\}$

$$\delta_I(n) = a_1\delta_I(n-1) + a_2\delta_I(n-2) + \epsilon(n) \qquad (2)$$

where $\{\epsilon(n)\}$ is a sequence of i.i.d. random variables. The mean of $\epsilon(n)$ is zero since the mean of $\delta_I(n)$ is zero by definition, and the variance of $\epsilon(n)$ is given by

$$\sigma_\epsilon^2 = \frac{(1+a_2)\left[(1-a_2)^2 - a_1^2\right]\sigma_\delta^2}{1-a_2} \qquad (3)$$

where σ_δ^2 is the variance of $\delta_I(n)$.

The long-range dependence is modeled using another second-order AR process for the mean sequence $M_I(n)$, or equivalently $\tilde{X}_I(j)$

$$\tilde{X}_I(j) = b_1\tilde{X}_I(j-1) + b_2\tilde{X}_I(j-2) + \theta(j) \qquad (4)$$

where $\{\theta(j)\}$ is a sequence of i.i.d. random variables. The mean and variance of $\theta(j)$ are determined as

$$\mu_\theta = (1-b_1-b_2)\tilde{\mu}_I \qquad (5)$$

and

$$\sigma_\theta^2 = \frac{(1+b_2)\left[(1-b_2)^2 - b_1^2\right]\tilde{\sigma}_I^2}{1-b_2} \qquad (6)$$

where $\tilde{\mu}_I$ and $\tilde{\sigma}_I^2$ are the mean and the variance of $\tilde{X}_I(j)$, respectively.

When generating traffic using the present model, once $\{\tilde{X}_I(j)\}$ is generated, $\{M_I(n)\}$ can be obtained by combining $\{\tilde{X}_I(j)\}$ with the scene-length sequence. Scene-length distribution is found to be modeled well by geometric distribution in the present study which confirms the results of [19] and [21]. We note that even though the same expression as in (1) was used in [19], the present approach differs from the one in [19] where the sequence $\{\tilde{X}_I(j)\}$ is modeled as a sequence of i.i.d. random variables (see comparison results in Section IV, Figs. 4–6). As in [19], we determine the order of the AR process in fitting $\delta_I(n)$ based on the *partial autocorrelation*

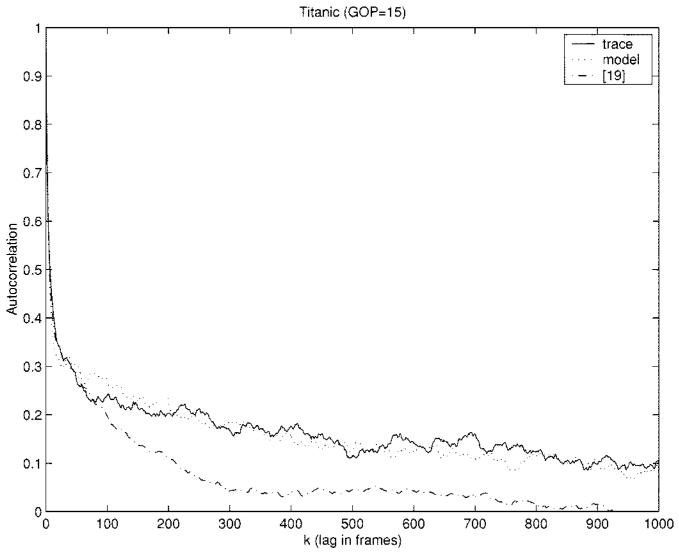

Fig. 4. Autocorrelation function of the I frame-size sequence.

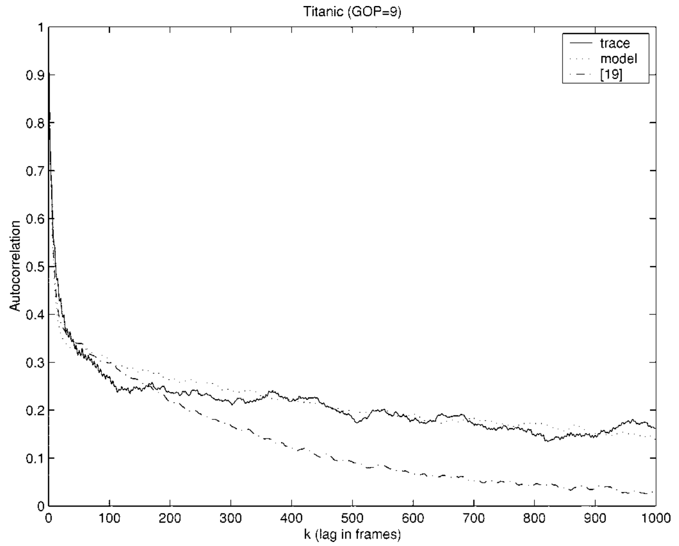

Fig. 5. Autocorrelation function of the I frame-size sequence.

function [3], which indicates that second-order AR process should be used. The same approach is employed to conclude that second-order AR process should also be used for $\tilde{X}_I(j)$. Due to the way that we generate $\{M_I(n)\}$ from $\{\tilde{X}_I(j)\}$, the two AR processes in (2) and (4) are not simply superposed to generate $X_I(n)$ in (1). Instead, they are nested with each other. We note that $\{\tilde{X}_I(j)\}$, generated by the AR process in (4), will be "stretched" unevenly according to a geometric distribution to generate the sequence $\{M_I(n)\}$.

In summary, we provide in the following a procedure for generating synthetic video frame-size sequences which model a given empirical video frame-size sequence using the present modeling approach.

Summary of Procedure for Generating Synthetic Video Traffic:

1) From the empirical video frame-size sequence, $\{X_{I,\,\mathrm{emp}}(n)\}$, $\{X_{P,\,\mathrm{emp}}(n)\}$, and $\{X_{B,\,\mathrm{emp}}(n)\}$ are obtained first for the I, P, and B frame-size sequences, respectively. The mean and the variance of

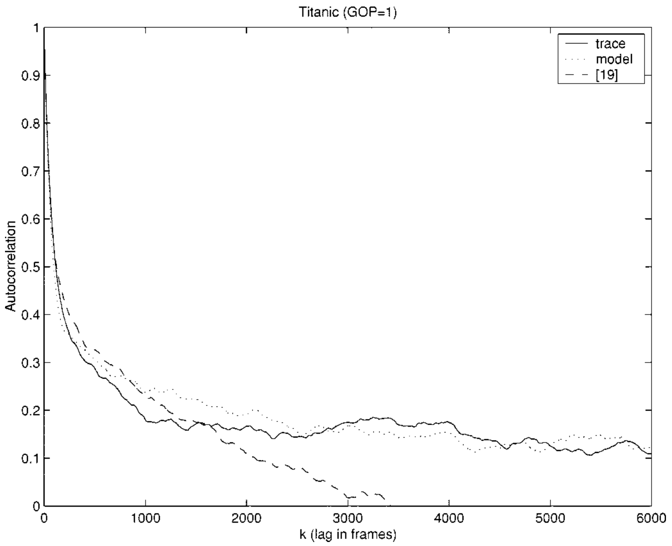

Fig. 6. Autocorrelation function of the (I) frame-size sequence.

the three sequences are estimated from $\{X_{I,\,\mathrm{emp}}(n)\}$, $\{X_{P,\,\mathrm{emp}}(n)\}$, and $\{X_{B,\,\mathrm{emp}}(n)\}$, respectively.

2) The scene detection is performed for $\{X_{I,\,\mathrm{emp}}(n)\}$ to obtain the measured scene mean sequence $\{M_{I,\,\mathrm{emp}}(n)\}$ and to obtain the scene-length sequence. A geometric distribution with parameter q, i.e.,

$$P\{N_j = k\} = (1-q)q^{k-1}, \qquad k = 1, 2, \ldots \tag{7}$$

where N_j denotes the length of the jth scene, is fitted for the scene-length sequence.

3) $\{\tilde{X}_{I,\,\mathrm{emp}}(j)\}$ is obtained from $\{M_{I,\,\mathrm{emp}}(n)\}$. The mean and the variance of $\tilde{X}_{I,\,\mathrm{emp}}(j)$ are estimated.

4) $\delta_{I,\,\mathrm{emp}}(n)$ is obtained as

$$\delta_{I,\,\mathrm{emp}}(n) = X_{I,\,\mathrm{emp}}(n) - M_{I,\,\mathrm{emp}}(n).$$

The variance of $\delta_{I,\,\mathrm{emp}}(n)$ is obtained and the mean of $\delta_{I,\,\mathrm{emp}}(n)$ should be zero or close to zero.

5) The parameters of the two AR processes are obtained using the least-square estimation given $\{\delta_{I,\,\mathrm{emp}}(n)\}$ to (2) and given $\{\tilde{X}_{I,\,\mathrm{emp}}(j)\}$ to (4), respectively.

6) The mean of $\epsilon(n)$ is set to zero while its variance is determined from (3) with σ_δ^2 chosen as the variance of $\delta_{I,\,\mathrm{emp}}(n)$. The mean and the variance are used to generate a sequence of i.i.d. random variables $\{\epsilon(n)\}$ with Normal distribution. The synthetic sequence $\{\delta_I(n)\}$ is then generated using (2).

7) The mean and the variance of $\theta(j)$ are determined from (5) and (6), with $\tilde{\mu}_I$ and $\tilde{\sigma}_I^2$ chosen as the mean and the variance of $\tilde{X}_{I,\,\mathrm{emp}}(j)$, respectively. $\{\theta(j)\}$ is generated similarly as $\{\epsilon(n)\}$ in Step 6. The synthetic sequence $\{\tilde{X}_I(j)\}$ is generated using (4). $\{\tilde{X}_I(j)\}$ can also be generated equivalently as follows. A sequence of i.i.d. zero mean random variables $\{\theta(j)\}$ with variance σ_θ^2 is used in (4) to generate zero mean random variables and then the mean $\tilde{\mu}_I$ is added to $\{\theta(j)\}$ to obtain $\{\tilde{X}_I(j)\}$.

8) The sequence $\{\tilde{X}_I(j)\}$ is combined with the scene-length distribution determined in Step 2 (i.e., a geometric distribution with parameter q) to generate

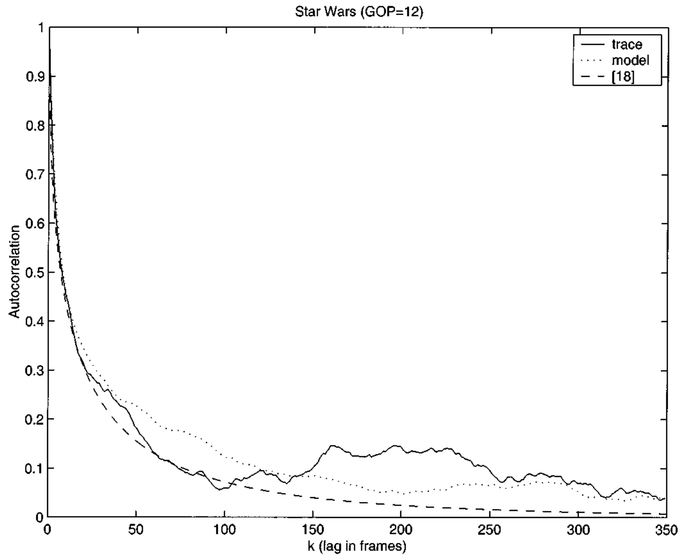

Fig. 7. Autocorrelation function of the I frame-size sequence.

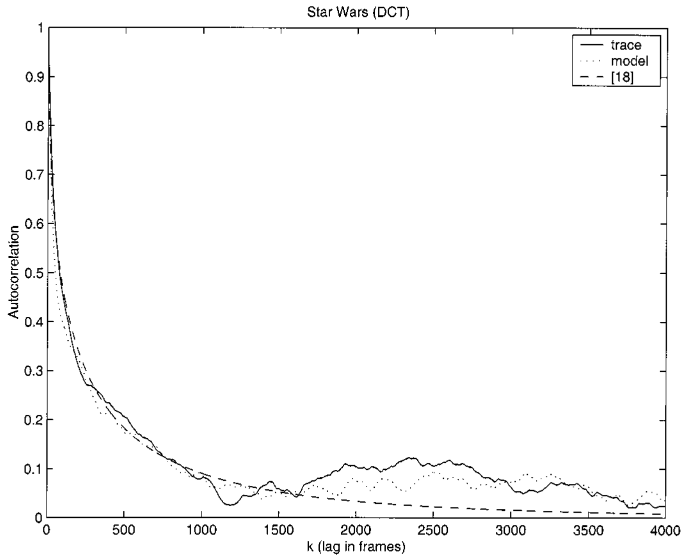

Fig. 8. Autocorrelation function of the frame-size sequence.

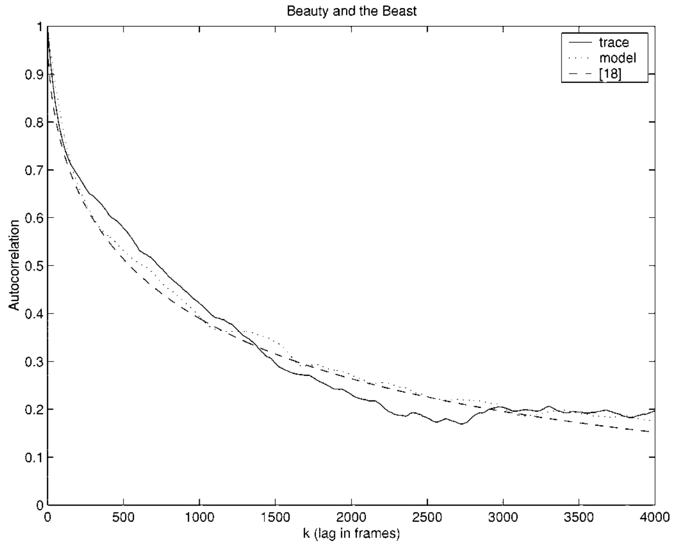

Fig. 9. Autocorrelation function of the frame-size sequence.

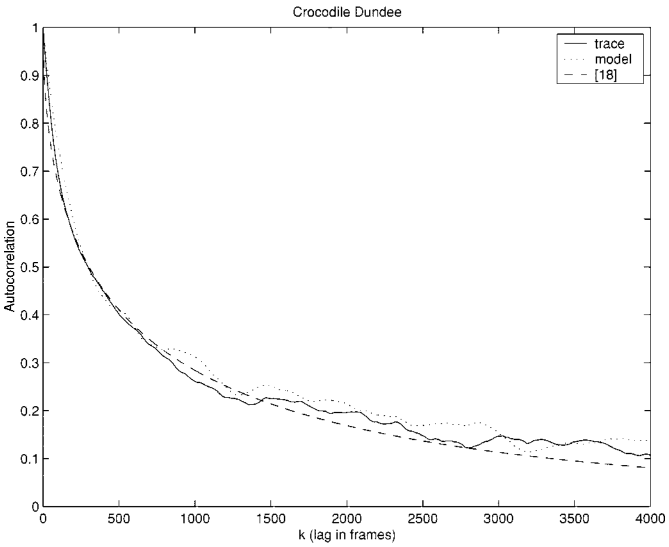

Fig. 10. Autocorrelation function of the frame-size sequence.

the sequence $\{M_I(n)\}$. The synthetic I frame-size sequence $\{X_I(n)\}$ is then generated as in (1).

9) The P and B frame-size sequences, $\{X_P(n)\}$ and $\{X_B(n)\}$, are generated using the mean and variance estimated from $\{X_{P,\,\mathrm{emp}}(n)\}$ and $\{X_{B,\,\mathrm{emp}}(n)\}$, respectively.

10) The generated I, P, and B frame-size sequences, $\{X_I(n)\}$, $\{X_P(n)\}$, and $\{X_B(n)\}$, are transformed to the hybrid Gamma/Pareto distribution (cf., Remark 3.2 below).

11) The I, P, and B frame-size sequences are combined together according to the chosen GOP pattern to form a synthetic video frame-size sequence $\{X(n)\}$.

Remark 3.2: To generate the I frame-size sequence with hybrid Gamma/Pareto distribution using AR process, an approach similar to that in [18] will be used. The inputs to (2) and (4) are chosen as i.i.d. random variables with Normal distribution. $\{X_I(n)\}$ is generated according to the procedure summarized above. $\{X_I(n)\}$ generated this way may have a distribution different from Normal due to the way $\{M_I(n)\}$ is generated. Furthermore, the parameters (i.e., the mean and the variance) of $\{X_I(n)\}$ will in general be different from the measured parameters. A transformation similar to that in [18] will be used to transform $\{X_I(n)\}$ to hybrid Gamma/Pareto distribution with estimated parameters. The present simulation results and the simulation results of [18] show that the autocorrelation functions before and after the transformation are almost identical to each other. The P and B frame-size sequences are first generated as i.i.d. random variables with estimated mean and variance (e.g., Normal distribution). They will then be transformed to hybrid Gamma/Pareto distribution. ■

C. Autocorrelation Structure for the I Frame Sequence

In the traffic-modeling literature, the term autocorrelation function is frequently used, and it is defined as the normalized autocovariance. For example, for the sequence $\{X_I(n)\}$,

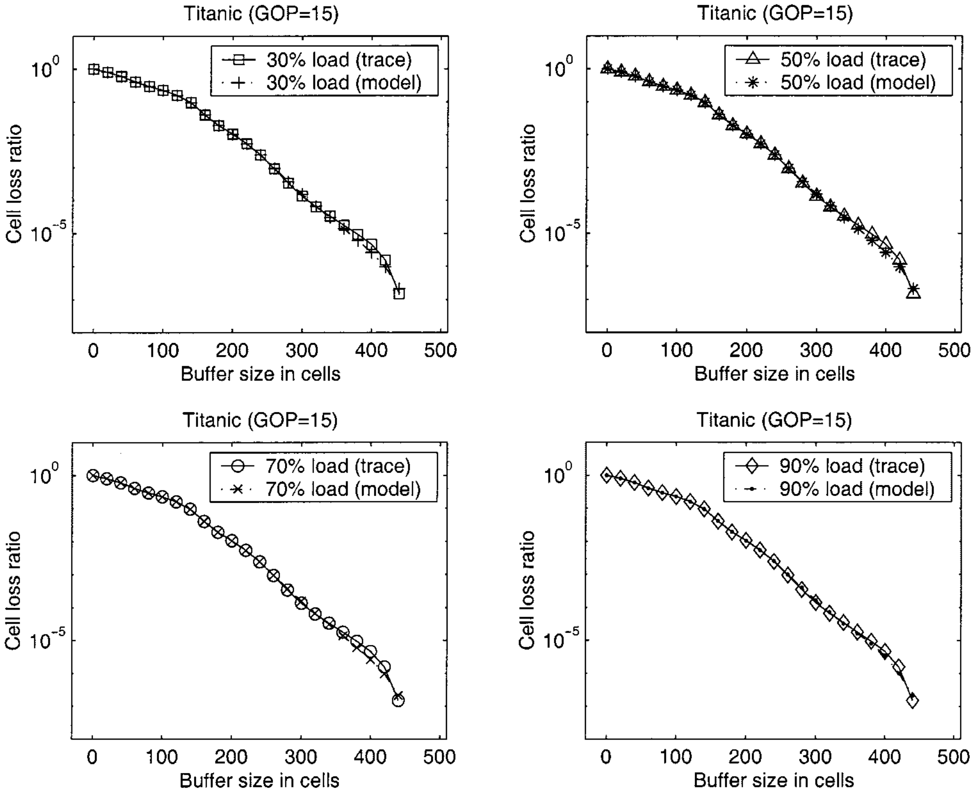

Fig. 11. Cell-loss ratio for single stream.

the definition of autocorrelation function used in the traffic modeling literature is given by

$$\rho_I(m) \triangleq \frac{E\{[X_I(n)-\mu_I][X_I(n+m)-\mu_I]\}}{\sigma_I^2} = \frac{E[X_I(n)X_I(n+m)]-\mu_I^2}{\sigma_I^2}$$

where μ_I and σ_I^2 are the mean and the variance of $\{X_I(n)\}$, respectively, and $m > 0$ is the index of frame lags. It is emphasized that all the processes are assumed to be stationary in the present paper (cf., Remark 3.1). From the stationarity property, $\rho_I(m)$ can also be written as

$$\rho_I(m) = \frac{E\{[X_I(1)-\mu_I][X_I(1+m)-\mu_I]\}}{\sigma_I^2} = \frac{E[X_I(1)X_I(1+m)]-\mu_I^2}{\sigma_I^2}. \tag{8}$$

It is well known that the autocorrelation function of $\{\delta_I(n)\}$ at lag m $(m > 0)$ is given by [3]

$$\rho_\delta(m) = \frac{\phi_1(1-\phi_2^2)\phi_1^m - \phi_2(1-\phi_1^2)\phi_2^m}{(\phi_1-\phi_2)(1+\phi_1\phi_2)} \tag{9}$$

where ϕ_1^{-1} and ϕ_2^{-1} are the roots of the characteristic equation of (2)

$$1 - a_1 s - a_2 s^2 = 0.$$

From (1), we have

$$\begin{aligned} E[X_I(1)X_I(1+m)] &= E\{[M_I(1)+\delta_I(1)][M_I(1+m)+\delta_I(1+m)]\} \\ &= E[M_I(1)M_I(1+m)] + E[\delta_I(1)\delta_I(1+m)] \end{aligned} \tag{10}$$

since $M_I(n)$ and $\delta_I(n)$ are independent and $\delta_I(n)$ has zero mean. The second term in (10) can easily be determined as

$$E[\delta_I(1)\delta_I(1+m)] = \rho_\delta(m)\sigma_\delta^2. \tag{11}$$

There are two cases that need to be considered for the first term in (10), i.e., when $M_I(1)$ and $M_I(1+m)$ are in the same scene and when they are in different scenes.

When $M_I(1)$ and $M_I(1+m)$ are in the same scene, i.e., $M_I(1) = M_I(1+m) = \tilde{X}_I(1)$, it is clear that

$$E[M_I(1)M_I(1+m)] = E\left[\tilde{X}_I^2(1)\right] = \tilde{\sigma}_I^2 + \tilde{\mu}_I^2.$$

Assume that the scene-length distribution follows a geometric distribution with parameter q given in (7). Then, it can be shown that the probability for $M_I(1)$ and $M_I(1+m)$ to be in the same scene is given by

$$P\{N_1 \geq 1+m\} = \sum_{k=m+1}^{\infty} P\{N_1 = k\} = \sum_{k=m+1}^{\infty} (1-q)q^{k-1} = q^m. \tag{12}$$

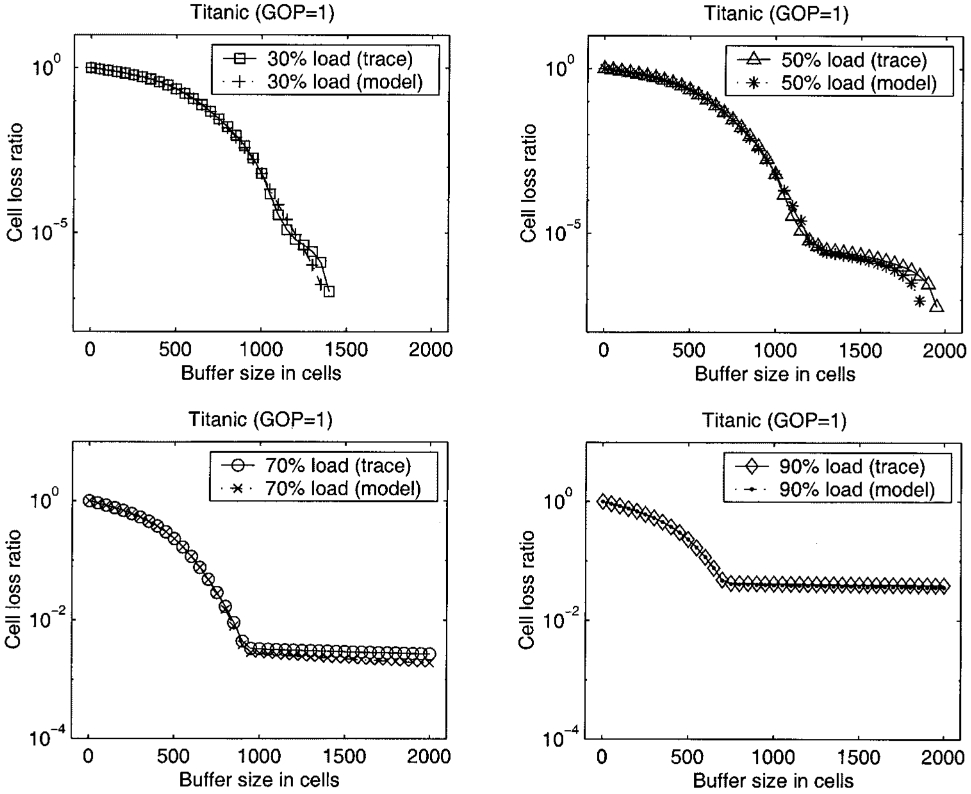

Fig. 12. Cell-loss ratio for single stream.

When $M_I(1)$ and $M_I(1+m)$ are in different scenes, without loss of generality, we assume that $M_I(1) = \tilde{X}_I(1)$ and $M_I(1+m) = \tilde{X}_I(1+l)$, where $1 \leq l \leq m$. In this case

$$E\left[M_I(1)M_I(1+m)\right] = E\left[\tilde{X}_I(1)\tilde{X}_I(1+l)\right] = \tilde{\rho}_I(l)\tilde{\sigma}_I^2 + \tilde{\mu}_I^2$$

and

$$\tilde{\rho}_I(l) = \frac{\psi_1(1-\psi_2^2)\psi_1^l - \psi_2(1-\psi_1^2)\psi_2^l}{(\psi_1-\psi_2)(1+\psi_1\psi_2)} \tag{13}$$

where ψ_1^{-1} and ψ_2^{-1} are the roots of the characteristic equation of (4). The probability for

$$\left\{M_I(1) = \tilde{X}_I(1) \quad \text{and} \quad M_I(1+m) = \tilde{X}_I(1+l)\right\}$$

i.e., $M_I(1)$ and $M_I(1+m)$ being separated by l scenes, is given by the following lemma.

Lemma 3.1: The probability of $M_I(1)$ and $M_I(1+m)$ being separated by l scenes, where $1 \leq l \leq m$, is given by

$$\begin{aligned} P_l(m) &= P\{N_1 + \ldots + N_{1+l} \geq 1+m \\ &\qquad \text{and} \quad N_1 + \ldots + N_l \leq m\} \\ &= (1-q)^l q^{m-l} \sum_{k=l}^{m} \left[\frac{1}{k!}\sum_{i=1}^{l}(-1)^{l-i}\binom{l}{i} i(i+1)\ldots \right. \\ &\qquad \left. (i+k-1)\right]. \end{aligned} \tag{14}$$

Proof: The probability generating function of N_j (i.e., geometric distribution with parameter q) is given by

$$\begin{aligned} G_N(z) &= E[z^{N_j}] = \sum_{k=1}^{\infty} P\{N_j = k\}z^k \\ &= \sum_{k=1}^{\infty}(1-q)q^{k-1}z^k = \frac{(1-q)z}{1-qz}. \end{aligned}$$

Fix l and denote $\xi = N_1 + N_2 + \ldots + N_l$. Note that ξ has minimum value of l. Also, note that ξ can be considered as a random variable composed of the sum of l random variables with the same distribution since the geometric distribution is memoryless; i.e., $\{N_j\}$ is a stationary process of i.i.d. random variables with a common geometric distribution. The probability generating function of ξ can be determined as

$$\begin{aligned} G_\xi(z) &= E[z^\xi] = E\left[z^{(N_1+\ldots+N_l)}\right] = (1-q)^l\left(\frac{z}{1-qz}\right)^l \\ &= \left(\frac{1-q}{q}\right)^l\left(\frac{1}{1-qz}-1\right)^l \\ &= \left(\frac{1-q}{q}\right)^l \sum_{i=0}^{l}(-1)^{l-i}\binom{l}{i}\frac{1}{(1-qz)^i}. \end{aligned} \tag{15}$$

From (15), the probability $P\{\xi = k\}$ can be determined as

$$P\{\xi = k\} = \frac{G_\xi^{(k)}(0)}{k!}$$

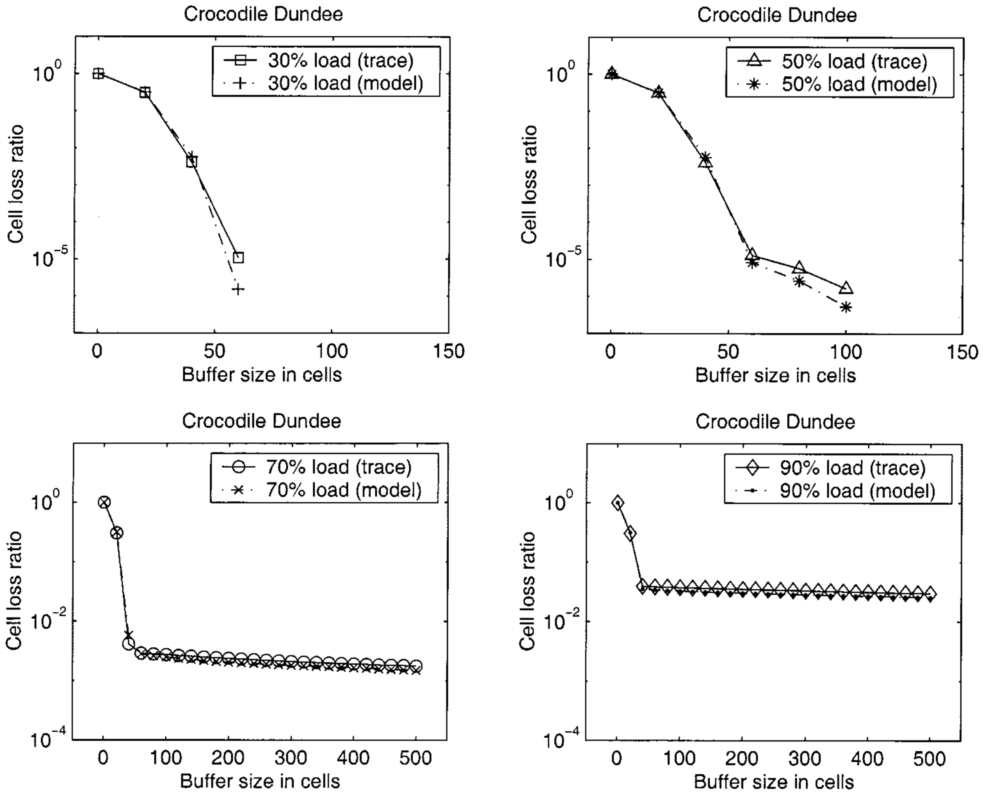

Fig. 13. Cell-loss ratio for single stream.

where $G_\xi^{(k)}$ denotes the kth derivative of G_ξ with

$$G_\xi^{(k)}(0) = 0, \qquad k = 1, 2, \ldots, l-1$$

and

$$\begin{aligned} G_\xi^{(k)}(0) = {}& \left(\frac{1-q}{q}\right)^l q^k \sum_{i=1}^{l} (-1)^{l-i}\binom{l}{i} \\ & \cdot i(i+1)\ldots(i+k-1), \\ & k = l, l+1, l+2, \ldots. \end{aligned}$$

Note that the summation starts from $i = 1$ since the term corresponding to $i = 0$ in (15) is a constant. Therefore

$$\begin{aligned} P_l(m) &= P\left\{M_I(1) = \tilde{X}_I(1) \right.\\ &\qquad \left. \text{and } M_I(1+m) = \tilde{X}_I(1+l)\right\} \\ &= P\{N_1 + \ldots + N_{l+1} \geq 1+m \\ &\qquad \text{and } N_1 + \ldots + N_l \leq m\} \\ &= \sum_{k=l}^{m} P\{N_1 + \ldots + N_{l+1} \geq 1 + m | \xi = k\} \\ &\quad \cdot P\{\xi = k\} \\ &= \sum_{k=l}^{m} P\{N_{l+1} \geq 1 + m - k\} P\{\xi = k\} \\ &= \sum_{k=l}^{m} \left[q^{m-k}\left(\frac{1-q}{q}\right)^l \frac{q^k}{k!} \sum_{i=1}^{l}(-1)^{l-i}\binom{l}{i} \right. \\ &\qquad \left. \cdot\, i(i+1)\ldots(i+k-1) \right] \\ &= (1-q)^l q^{m-l} \sum_{k=l}^{m} \\ &\quad \cdot \left[\frac{1}{k!}\sum_{i=1}^{l}(-1)^{l-i}\binom{l}{i} i(i+1)\ldots(i+k-1)\right] \end{aligned}$$

for $l = 1, 2, \ldots, m$, where

$$P\{N_{l+1} \geq 1 + m - k\} = q^{m-k}$$

can be shown similarly as (12). Note that the summations in the above start from $k = l$ because $\xi = N_1 + \ldots + N_l$ has a minimum value of l. ■

In summary, the first term in (10) is determined as

$$\begin{aligned} & E[M_I(1)M_I(1+m)] \\ &= \begin{cases} \tilde{\sigma}_I^2 + \tilde{\mu}_I^2 & w.p.\ q^m \\ \tilde{\rho}_I(l)\tilde{\sigma}_I^2 + \tilde{\mu}_I^2 & w.p.\ P_l(m) \text{ in (14) for } l = 1, 2, \ldots, m \end{cases} \end{aligned} \tag{16}$$

The following proposition can now be given.

Proposition 3.1: Let $\rho_I(m)$ be the autocorrelation function for $\{X_I(n)\}$ at lag m. Then

$$\rho_I(m) = \frac{\rho_\delta(m)\sigma_\delta^2 + q^m \tilde{\sigma}_I^2 + \tilde{\sigma}_I^2 \sum_{l=1}^{m} P_l(m)\tilde{\rho}_I(l)}{\sigma_I^2}$$

where $\rho_\delta(m)$ and $\tilde{\rho}_I(l)$ are given in (9) and (13), respectively.

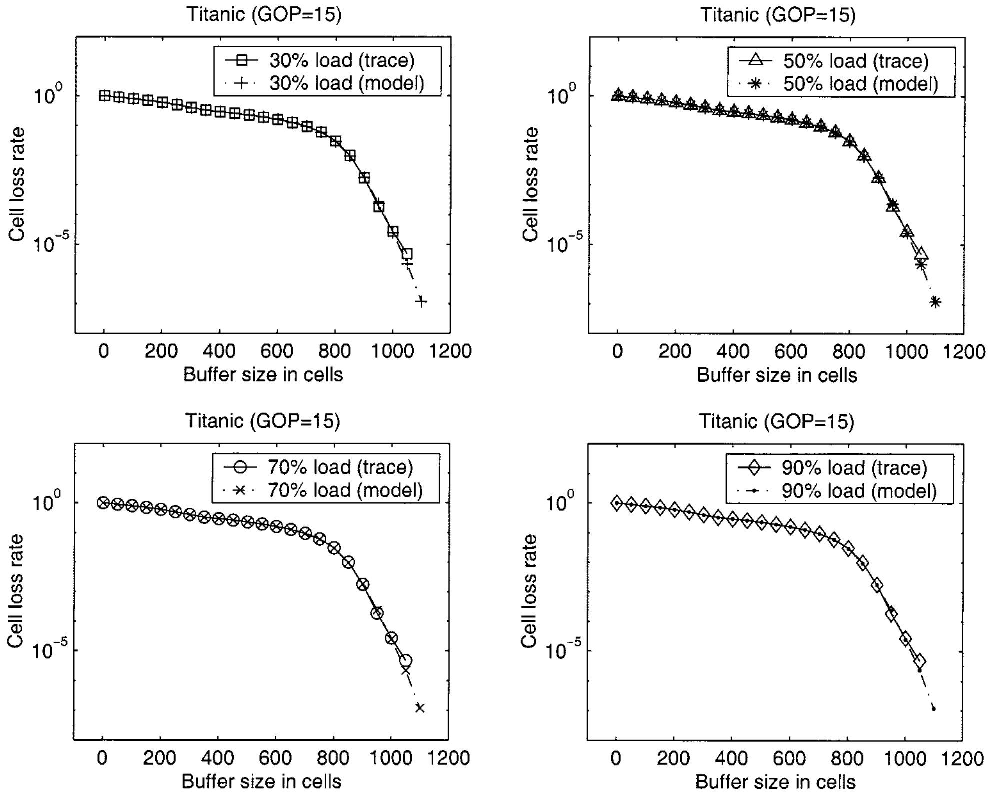

Fig. 14. Cell-loss ratio for five homogeneous multiplexed streams.

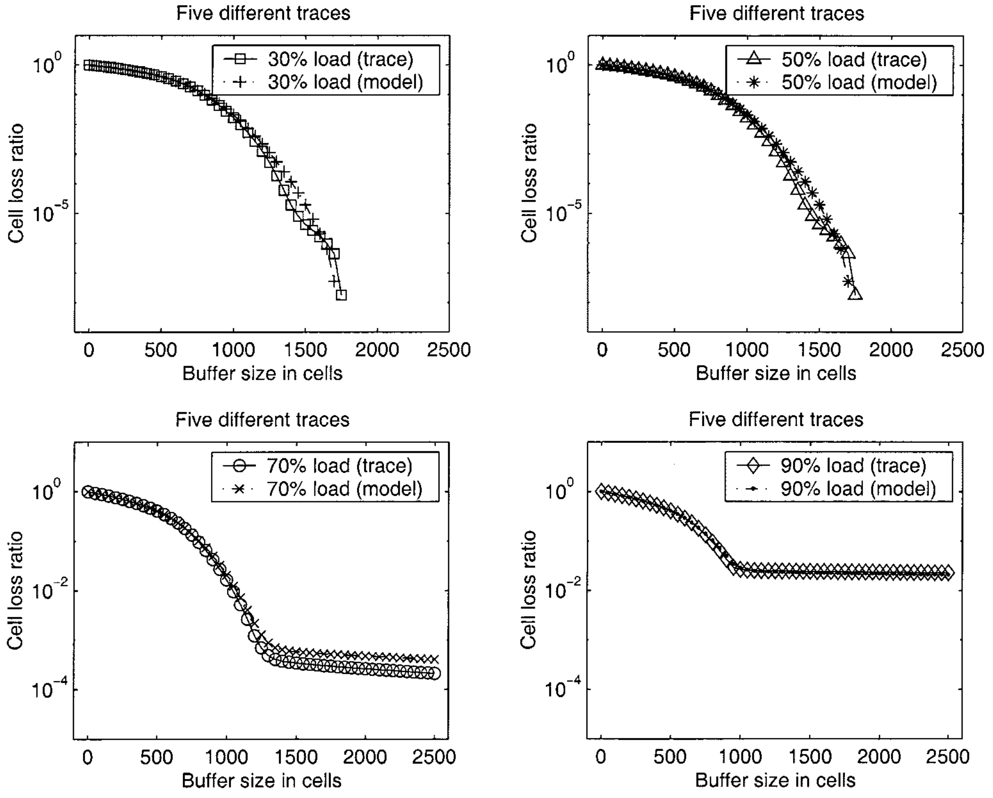

Fig. 15. Cell-loss ratio for five heterogeneous multiplexed streams.

Proof: Combining (8), (10), (11), and (16), we obtain

$$\rho_I(m) = \left[\rho_\delta(m)\sigma_\delta^2 + q^m(\tilde{\sigma}_I^2 + \tilde{\mu}_I^2) + \sum_{l=1}^{m} P_l(m)(\tilde{\rho}_I(l)\tilde{\sigma}_I^2 + \tilde{\mu}_I^2) - \mu_I^2\right] \Big/ \sigma_I^2.$$

The probability of $M_I(1)$ and $M_I(1+m)$ in the same scene is shown to be q^m. The probability of $M_I(1)$ and $M_I(1+m)$ in different scenes should be $1-q^m$ which must equal the sum of $P_l(m)$, i.e.,

$$\sum_{l=1}^{m} P_l(m) = 1 - q^m.$$

Note that $P_l(m)$ is only valid for $l = 1, 2, \ldots, m$, and $l = 0$ indicates that $M_I(1)$ and $M_I(1+m)$ are in the same scene. $\rho_I(m)$ can then be rewritten as

$$\rho_I(m) = \left[\rho_\delta(m)\sigma_\delta^2 + q^m(\tilde{\sigma}_I^2 + \tilde{\mu}_I^2) + \tilde{\sigma}_I^2 \sum_{l=1}^{m} P_l(m)\tilde{\rho}_I(l) + (1-q^m)\tilde{\mu}_I^2 - \mu_I^2\right] \Big/ \sigma_I^2$$

$$= \frac{\rho_\delta(m)\sigma_\delta^2 + q^m\tilde{\sigma}_I^2 + \tilde{\sigma}_I^2 \sum_{l=1}^{m} P_l(m)\tilde{\rho}_I(l) + (\tilde{\mu}_I^2 - \mu_I^2)}{\sigma_I^2}.$$

It can be shown that $\mu_I = \tilde{\mu}_I$ (cf., next Remark) which leads to the proof of the proposition. ■

Remark 3.3: It is shown in [19] that $M_I(n)$ and $\tilde{X}_I(j)$ have the same distribution. What is needed in our proof of Proposition 3.1 is that $M_I(n)$ [or equivalently $X_I(n)$, since $\delta_I(n)$ has zero mean] and $\tilde{X}_I(j)$ have the same mean. The proof for $\mu_I = \tilde{\mu}_I$ can easily be done based on the stationarity assumption made in the present paper. ■

IV. Simulation Results

We have implemented a procedure for generating the statistics of MPEG encoded video frame-size sequences. In the first stage, the video sequences from video tapes are captured using the SunVideo card in a Sun Sparc 20 workstation and converted to YUV format. They will then be encoded with specified parameters and patterns with a chosen MPEG-2 encoder. The MPEG-2 encoder used in the present experiments is the implementation of the MPEG Software Simulation Group.[1] This encoder has been updated with the latest changes in the MPEG-2 standard. There are a number of parameters that can be configured, but in the present experiments, we only try different GOP patterns. Other configurable MPEG-2 parameters are set to provide the least constraints on the MPEG streams for best picture quality. No enhancement layers for MPEG-2 encoding will be considered and only base layer streams will be used in the present study.

TABLE I
Titanic Traces

Trace (GOP size)	Titanic (GOP=15)	Titanic (GOP=9)	Titanic (GOP=1)
a_1	0.7109	0.7977	0.8707
a_2	0.0556	0.0382	0.1126
b_1	0.5327	0.2360	0.3365
b_2	0.1468	0.3034	0.2424
$\tilde{\mu}_I$	187	179	553
$\tilde{\sigma}_I$	29	25	112
μ_δ	0.0	0.0	0.0
σ_δ	36	34	121
μ_P	160	157	N/A
σ_P	13	14	N/A
μ_B	67	66	N/A
σ_B	9	10	N/A

To demonstrate the applicability of the present modeling approach to MPEG-2 video sources with different GOP sizes, the movie Titanic is used. Based on the above set-up, 333 720 frames have been recorded from the movie Titanic. This represents slightly more than three hours with a 30 frames/second (fps) frame rate used in the capturing. The frames are encoded with different GOP sizes and the frame sizes are recorded. The GOP sizes chosen in the encoding are 1 (I frames only), 9 ($IBBPBBPBB$), and 15 ($IBBPBBPBBPBBPBB$).

The frame-size distribution obtained from empirical sequences confirms the choice made earlier, i.e., the hybrid Gamma/Pareto distribution for all three types of frame-size sequences. In Table I, we show the estimates of various parameters in the model (where μ_P (μ_B) and σ_P (σ_B) are the mean and the standard deviation of the P (B) frame-size sequence, respectively). The unit used in the present paper for the frame size is cell which is equivalent to the payload of an ATM cell (i.e., 384 data bits). It is noted that a_1 and a_2 (also b_1 and b_2) in Table I all satisfy the stationarity condition, i.e., the roots of the characteristic equations of (2) and (4) lie outside the unit circle (cf., [3]). The roots of the characteristic equations of (2) and (4) for each case in Table I are also real. The simulation study in this section will examine the correlation structure of the traffic generated using the present modeling approach and compare it to that of empirical video frame-size sequences. Since traffic correlation may have a large impact on queueing behavior, the simulation results here will provide certain indications for the appropriateness of the present modeling approach. The autocorrelation functions of the frame-size sequences generated using the present model are compared to the autocorrelation functions of Titanic empirical traces in Figs. 4–6. Clearly, the present model provides a very good match for the autocorrelation functions between the real traffic and the model generated traffic, at both small and large lags.

We also compare the result of [19] to the present approach in Figs. 4–6. As we have pointed out earlier, in [19], the sequence $\{\tilde{X}_I(j)\}$ for $M_I(n)$ in (1) is modeled as a sequence of i.i.d. random variables. The results in Figs. 4–6 show that [19]

[1] cf., http://www.mpeg2.de/video/software

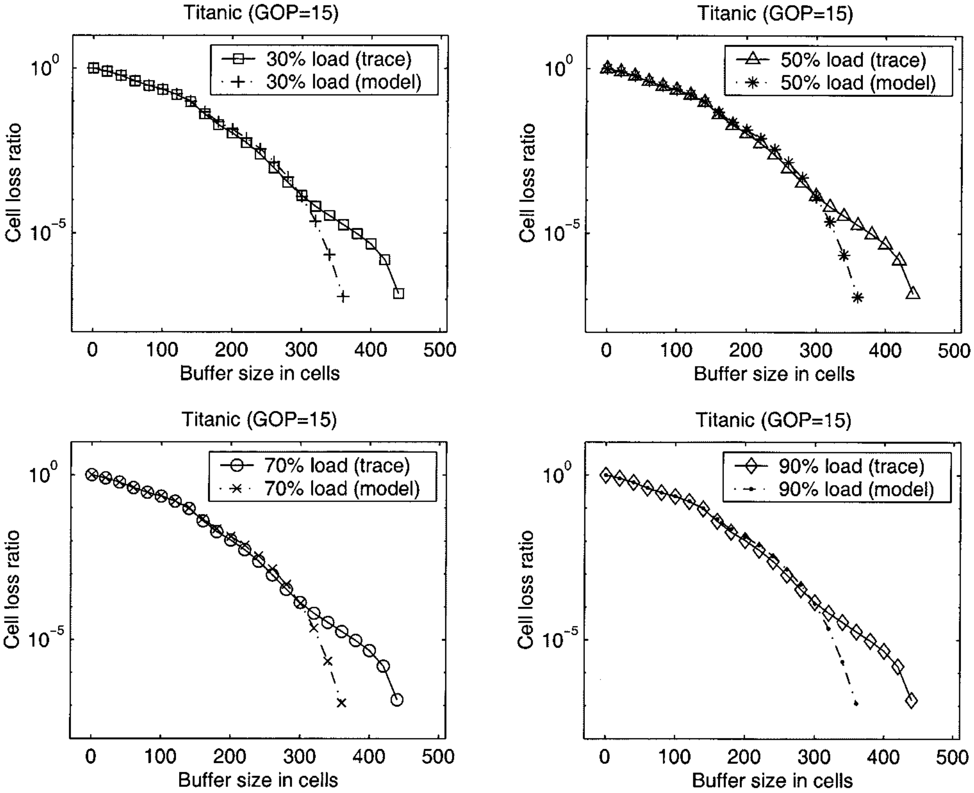

Fig. 16. Comparison of cell-loss ratios between the empirical trace and the model generated trace (without transforming to Gamma/Pareto distribution).

TABLE II
OTHER PUBLICLY AVAILABLE TRACES

Movie	Source	Trace Length (frames)	Compression Scheme
Star Wars	[9]	174,136	MPEG-1 (GOP=12)
Star Wars	[9]	171,000	DCT
Beauty and the Beast	[6]	143,442	JPEG
Crocodile Dundee	[6]	168,565	JPEG

matches well the empirical autocorrelation functions at small lags, but misses the autocorrelation functions at large lags.

To test the present modeling approach for video sources with diverse content, we utilize several public domain video traces. The traces are listed in Table II.

Traces encoded using DCT and JPEG are treated as MPEG sequences with no P and B frames (i.e., the GOP size is 1). The autocorrelation functions of the traffic generated using the present model are compared to the autocorrelation functions of empirical traces in Figs. 7–10. The results of [18] are also shown in the figures, where the autocorrelation functions have the form given by $e^{-\beta\sqrt{k}}$ with $\beta > 0$. Again, the present model provides a very good match for the autocorrelation function at all lags shown in the figures.

We note that the results of [18] also provide very good match for the autocorrelation function in the experiments. However, the present model provides slightly better results for the Star Wars traces (cf., Figs. 7 and 8).

V. QUEUEING PERFORMANCE STUDY

To further verify the appropriateness of the present video traffic model, we will study its queueing performance and compare it to that of the empirical traces. While a good traffic model is expected to capture some statistical properties of the underlying empirical data trace, the ultimate goal is to predict network performance accurately for the purpose of dimensioning network resources. The queueing performance should be deemed as a crucial factor that determines the appropriateness of a traffic model [18].

The queueing system utilized in the present study consists of a single-server first-in first-out queue with a finite buffer (size in cells). The release rate (or bandwidth, in cells per second) is a constant to be determined according to the desired load condition. To simulate an ATM multiplexer, data streams will be buffered before transmitting to the outgoing link [28]. Two types of simulation studies are conducted, i.e., single stream and multiplexed streams.

In the single-stream case, the cell-loss ratio is examined at four different loads, i.e., U =30% (light load), U =50% (moderate load), U =70% (heavy load), and U =90% (very heavy load). In the present paper, we define the traffic load as the ratio between the mean cell rate of the (aggregate) traffic and the bandwidth (or the release rate). The algorithm used in [18] for approximating the cell-loss ratio is modified to approximate the performance of an ATM multiplexer. In all four cases, the simulations are run for buffer size equal to zero incremented with a fixed step size in cells (e.g., 20 or 50 cells). Ten independent simulations are used, each starting at a different location in the

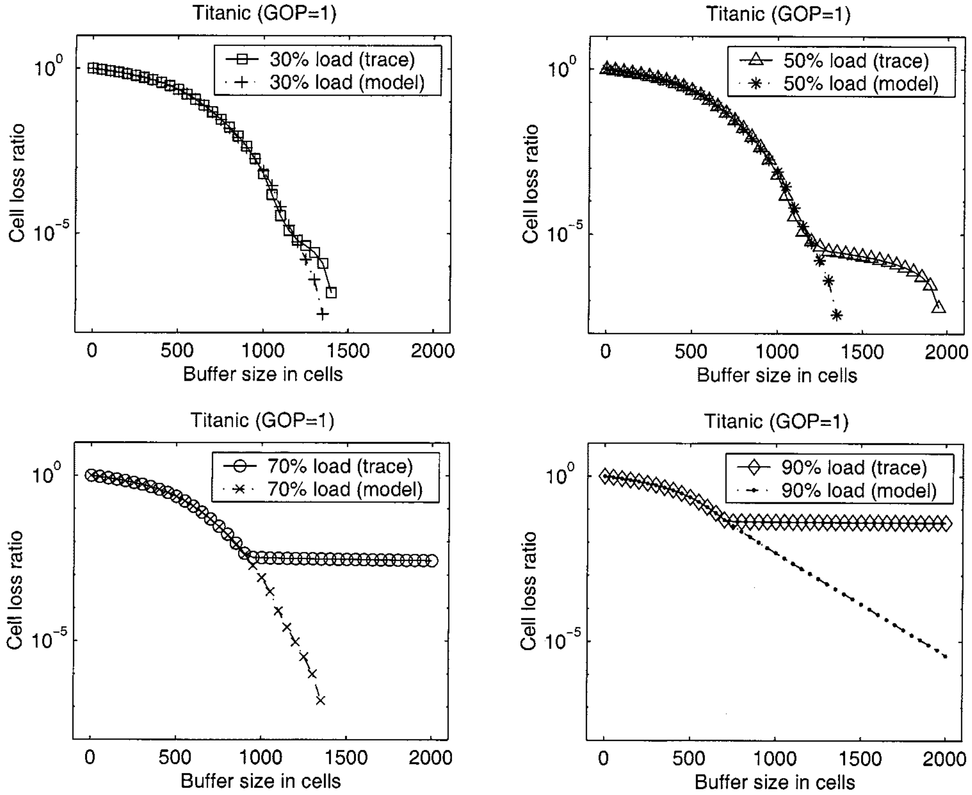

Fig. 17. Comparison of cell-loss ratios between the empirical trace and the model generated trace (with no autocorrelation).

trace. The average cell-loss ratio over the ten simulation runs are displayed in Fig. 11 (for GOP =15) and Fig. 12 (for GOP =1). Except for a few occasions, for each of the four loads chosen, the ten simulation runs provide exactly the same cell-loss prediction. We can see that the present model provides very close predictions of cell-loss ratios compared to that of the empirical streams. We conclude that the present model provides very good performance predictions at various loads for a large range of buffer sizes. We can also see from Fig. 12 that when the traffic is less bursty (i.e., when GOP $= 1$) and the traffic load is high, there exists a largest buffer size beyond which increasing the buffer size would not reduce the cell-loss ratio [28].

The simulation results reported above are only for the Titanic traces with GOP $= 15$ and GOP $= 1$. Performance studies have also been conducted for all of the traces listed in Tables I and II; all of these experiments show similar results to those in Figs. 11 and 12 for cell-loss predictions. We will display only one of them in Fig. 13 for the JPEG trace of Crocodile Dundee and the rest will not be displayed due to space limitations.

For homogeneous multiplexed streams, the frame-size sequence of the movie Titanic (GOP =15) is broken down into five subsequences with each having the same length. The five subsequences will then be multiplexed and its queueing performance will be studied. This procedure simulates the multiplexing of homogeneous traces. Again, ten independent simulations are used, each starting at a different location in the trace. The average cell-loss ratio over the ten simulation runs are displayed in Fig. 14. We can see that the present model provides very close predictions of cell-loss ratio compared to that of the multiplexed empirical stream. The purpose of the present simulation for multiplexed video streams is not to show how the multiplexing should be done. Instead, the purpose is to show the accuracy of the present modeling approach in predicting the cell-loss ratio under certain conditions. We note that the five streams in the multiplexing are not synchronized, i.e., the I frames from one stream will not coincide in time with I frames from any other streams; thus, the aggregate traffic is smoother than the individual streams. Exactly the same arrangements in multiplexing are used for both the synthetic streams and the empirical streams; they are arranged according to [19] to achieve an "optimal" arrangement. The multiplexed streams are aligned such that a GOP of the first source is one frame lag from a GOP of the second source, a GOP of the second source is one frame lag from a GOP of the third source, and so on (cf., [19]).

Our next simulation result is for heterogeneous multiplexed streams, where we multiplex the following five different traces: Titanic GOP $= 1$, Titanic GOP $= 9$, Star Wars GOP $= 12$, Beauty and the Beast, and Crocodile Dundee. The results are shown in Fig. 15, where very good queueing performance prediction is demonstrated again for different loads and for a large range of buffer sizes.

To determine the effects of the probability distribution of frame sizes and the autocorrelation structure of I frame-size sequence on the queueing performance, we conduct the following comparison study. In the first set of experiments, frame sizes are generated as in the procedure summarized in Section III-B, except Step 10 (transforming to the hybrid Gamma/Pareto distribution) which will not be performed. Thus, the frame-size sequence will have the correct autocorrelation structure but without the correct probability distribution. The results are shown in Fig. 16, where we can see that the empirical traces and the model generated traces perform similarly until the buffer size reaches 300 cells. In the second set of experiments, frame sizes for the three types of frames are generated as sequences of i.i.d. random variables and converted to the hybrid Gamma/Pareto distribution. The frame-size sequence in this case will have the correct probability distribution but without the correct correlation. The results are shown in Fig. 17, where we can see that the empirical traces and the model generated traces perform drastically different for large buffers when the load is high.

We note that the results in Fig. 16 are for GOP $=15$ and the results in Fig. 17 are for GOP $= 1$. The same experiments as the ones in Fig. 17 are also conducted for GOP $=15$; and the same experiments as the ones in Fig. 16 are also conducted for GOP $=1$. However, in both cases, the empirical traces and the model generated traces perform very closely to each other (similar to Figs. 11 and 12). Intuitively, these phenomena can be explained as follows. When the traffic is very bursty (e.g., when GOP $=15$), cell losses happen most likely at the traffic bursts (large sizes in the frame-size sequence). It is the correct frame-size distribution, i.e., the correct tail behavior provided by the hybrid Gamma/Pareto distribution, that guarantees to generate the large sizes in the frame-size sequence; in this case, the correct frame-size distribution will over shadow the autocorrelation between frame sizes in predicting the cell-loss ratio. When the traffic is less bursty (e.g, when GOP $=1$), the correct tail behavior is not important any more in predicting the cell-loss ratio, since large sizes in the traffic stream appear almost all the time; in this case, cell losses will show more reliance on the autocorrelation between frame sizes. Based on these experiments, we conclude that both the marginal distribution of frame sizes and the autocorrelation structure are important in predicting queueing performance such as cell-loss ratio and their effects vary according to the burstiness of the video traffic. When the video trace is very bursty (e.g., GOP$=15$), the correct marginal distribution (i.e., the hybrid Gamma/Pareto distribution) of frame sizes is more important than the autocorrelation structure in queueing performance predictions. When the video trace is less bursty (e.g., GOP $=1$), the correct autocorrelation structure is more important than the marginal distribution in queueing performance predictions.

VI. Conclusion

In the present paper, a modeling approach based on nested AR processes is developed for MPEG video traffic streams. One AR process is used to model the mean size of each traffic scene which provides a constant value for the mean of all the frames in a scene. The length of each scene is modeled by a geometric distribution. This AR process is thus stretched unevenly according to the geometric distribution, and it contributes to the long-range dependence in the autocorrelation structure. Another AR process is used to model the fluctuations about the mean of each traffic scene. This AR process contributes to the matching for short range dependence in the autocorrelation structure. Simulation results show that the present model provides very good match for the autocorrelation function between the real traffic and the model generated video traffic, at both small and large lags. Empirical traces used include video streams encoded using MPEG-2, MPEG-1, JPEG, and DCT schemes (JPEG/DCT streams are treated the same way as MPEG streams with GOP size equal to 1). Study of queueing performance is conducted for single stream and multiplexed streams. The results show that the present model provides appropriate predictions for the actual cell-loss ratio under various buffer sizes and different load conditions, for both single stream and multiplexed streams. A comparison study is also conducted which shows that both the correct marginal distribution of frame sizes and the autocorrelation structure are needed for good queueing performance predictions. In particular, it is demonstrated through examples that when the traffic is very bursty, the correct marginal distribution is crucial in predicting the cell-loss ratio, and when the traffic is less bursty, the correct autocorrelation structure is crucial in predicting the cell-loss ratio.

References

[1] A. Adas, “Traffic models in broadband networks,” *IEEE Commun. Mag.*, vol. 35, pp. 82–89, July 1997.

[2] J. Beran, R. Sherman, M. S. Taqqu, and W. Willinger, “Long-range dependence in variable-bit-rate video traffic,” *IEEE Trans. Commun.*, vol. 43, pp. 1566–1579, Feb./Mar./Apr. 1995.

[3] G. E. P. Box and G. M. Jenkins, *Time Series Analysis: Forecasting and Control*. San Francisco, CA: Holden-Day, 1976.

[4] P.-R. Chang and J.-T. Hu, “Optimal nonlinear adaptive prediction and modeling of MPEG video in ATM networks using pipelined recurrent neural networks,” *IEEE J. Select. Areas Commun.*, vol. 15, pp. 1087–1100, Aug. 1997.

[5] A. M. Dawood and M. Ghanbari, “Content-based MPEG video traffic modeling,” *IEEE Trans. Multimedia*, vol. 1, pp. 77–87, Mar. 1999.

[6] W. Feng, “Video-on-demand services: Efficient transportation and decompression of variable bit rate video,” Ph.D. dissertation, Univ. Michigan, Ann Arbor, MI, Apr. 1996.

[7] M. R. Frater, J. F. Arnold, and P. Tan, “A new statistical model for traffic generated by VBR coders for television on the broadband ISDN,” *IEEE Trans. Circuits Syst. Video Technol.*, vol. 4, pp. 521–526, Dec. 1994.

[8] V. S. Frost and B. Melamed, “Traffic modeling for telecommunications networks,” *IEEE Commun. Mag.*, vol. 32, pp. 70–81, Mar. 1994.

[9] M. W. Garrett and W. Willinger, “Analysis, modeling and generation of self-similar VBR video traffic,” *Computer Commun. Rev.*, vol. 24, pp. 269–280, 1994.

[10] M. Grossglauser and J.-C. Bolot, “On the relevance of long-range dependence in network traffic,” *Computer Commun. Review*, vol. 26, pp. 15–24, 1996.

[11] R. Grünenfelder, J. P. Cosmas, S. Manthorpe, and A. Odinma-Okafor, “Characterization of video codecs as autoregressive moving average processes and related queueing system performance,” *IEEE J. Select. Areas Commun.*, vol. 9, pp. 284–293, Apr. 1991.

[12] B. G. Haskell, A. Puri, and A. N. Netravali, *Digital Video: An Introduction to MPEG-2*. New York: Chapman & Hall, 1997.

[13] D. P. Heyman and T. V. Lakshman, “Source models for VBR broadcast-video traffic,” *IEEE Trans. Networking*, vol. 4, pp. 40–48, Feb. 1996.

[14] D. P. Heyman, A. Tabatabai, and T. V. Lakshman, “Statistical analysis and simulation study of video teleconference traffic in ATM networks,” *IEEE Trans. Circuits Syst. Video Technol.*, vol. 2, pp. 49–59, Mar. 1992.

[15] C. Huang, M. Devetsikiotis, I. Lambadaris, and A. R. Kaye, “Modeling and simulation of self-similar variable bit rate compressed video: A unified approach,” *Computer Commun. Rev.*, vol. 25, pp. 114–125, 1995.

[16] B. Jabbari, F. Yegenoglu, Y. Kuo, S. Zafar, and Y.-Q. Zhang, “Statistical characterization and block-based modeling of motion-adaptive coded video,” *IEEE Trans. Circuits Syst. Video Technol.*, vol. 3, pp. 199–207, June 1993.

[17] P. R. Jelenković, A. A. Lazar, and N. Semret, "The effect of multiple time scales and subexponentiality in MPEG video streams on queueing behavior," *IEEE J. Select. Areas Commun.*, vol. 15, pp. 1052–1071, Aug. 1997.

[18] M. M. Krunz and A. M. Makowski, "Modeling video traffic using $M/G/\infty$ input processes: A compromise between Markovian and LRD models," *IEEE J. Select. Areas Commun.*, vol. 16, pp. 733–748, June 1998.

[19] M. Krunz and S. K. Tripathi, "On the characterization of VBR MPEG streams," *Perform. Eval. Rev.*, vol. 25, pp. 192–202, 1997.

[20] A. La Corte, A. Lombardo, S. Palazzo, and S. Zinna, "Modeling activity in VBR video sources," *Signal Processing: Image Commun.*, vol. 3, pp. 167–178, June 1991.

[21] A. A. Lazar, G. Pacifici, and D. E. Pendarakis, "Modeling video sources for real-time scheduling," *Multimedia Syst.*, vol. 1, pp. 253–266, 1994.

[22] B. Maglaris, D. Anastassiou, P. Sen, G. Karlsson, and J. D. Robbins, "Performance models of statistical multiplexing in packet video communications," *IEEE Trans. Commun.*, vol. 36, pp. 834–844, July 1988.

[23] N. M. Marafih, Y.-Q. Zhang, and R. L. Pickholtz, "Modeling and queueing analysis of variable-bit-rate coded video sources in ATM networks," *IEEE Trans. Circuits Syst. Video Technol.*, vol. 4, pp. 121–128, Apr. 1994.

[24] H. Michiel and K. Laevens, "Teletraffic engineering in a broad-band era," *Proc. IEEE*, vol. 85, pp. 2007–2033, Dec. 1997.

[25] M. Nomura, T. Fujii, and N. Ohta, "Basic characteristics of variable rate video coding in ATM environment," *IEEE J. Select. Areas Commun.*, vol. 7, pp. 752–760, June 1989.

[26] B. Porat, *Digital Processing of Random Signals*. Englewood Cliffs, NJ: Prentice-Hall, 1994.

[27] O. Rose, "Simple and efficient models for variable bit rate MPEG video traffic," *Performance Evaluation*, vol. 30, pp. 69–85, 1997.

[28] M. Schwartz, *Broadband Integrated Networks*. Englewood Cliffs, NJ: Prentice Hall, 1996.

[29] P. Sen, B. Maglaris, N.-E. Rikli, and D. Anastassiou, "Models for packet switching of variable-bit-rate video sources," *IEEE J. Select. Areas Commun.*, vol. 7, pp. 865–869, June 1989.

[30] C. Shim, I. Ryoo, J. Lee, and S. Lee, "Modeling and call admission control algorithm of variable bit rate video in ATM networks," *IEEE J. Select. Areas Commun.*, vol. 12, pp. 332–344, Feb. 1994.

[31] N. Shroff and M. Schwartz, "Characterizing highly correlated video traffic in high-speed asynchronous transfer mode networks," *J. Electron. Imaging*, vol. 5, pp. 144–158, Apr. 1996.

[32] P. Skelly, M. Schwartz, and S. Dixit, "A histogram-based model for video traffic behavior in an ATM multiplexer," *IEEE Trans. Networking*, vol. 1, pp. 446–459, Aug. 1993.

[33] S. Xu and Z. Huang, "A gamma autoregressive video model on ATM networks," *IEEE Trans. Circuits Syst. Video Technol.*, vol. 8, pp. 138–142, Apr. 1998.

[34] F. Yegenoglu, B. Jabbari, and Y.-Q. Zhang, "Motion-classified autoregressive modeling of variable bit rate video," *IEEE Trans. Circuits Syst. Video Technol.*, vol. 3, pp. 42–53, Feb. 1993.

[35] *Coding of Moving Pictures and Associated Audio for Digital Storage Media up to 1.5Mbits/s—Part 2: Video*, International Standard: ISO/IEC IS 11 172-2, 1993.

[36] *Coding of Moving Pictures and Associated Audio—Part 2: Video, I*, International Standard: ISO/IEC IS 13818-2, 1994.

Derong Liu (S'91–M'94–SM'96) received the Ph.D. degree in electrical engineering from the University of Notre Dame, Notre Dame, IN, in 1994.

From 1993 to 1995, he was with General Motors Research and Development Center, Warren, MI, where he worked in automotive engine diagnostics. From 1995 to 1999, he was Assistant Professor in the Department of Electrical and Computer Engineering, Stevens Institute of Technology, Hoboken, NJ. Currently, he is an Assistant Professor in the Department of Electrical Engineering and Computer Science, University of Illinois, Chicago, IL. He is coauthor (with A. N. Michel) of the book *Dynamical Systems with Saturation Nonlinearities: Analysis and Design* (New York: Springer-Verlag, 1994).

Dr. Liu served as an Associate Editor for IEEE TRANSACTIONS ON CIRCUITS AND SYSTEMS—I: FUNDAMENTAL THEORY AND APPLICATIONS during 1997–1999. He was a Member of the Program Committees of the 11th IEEE International Symposium on Intelligent Control (1996) and the 14th IEEE International Symposium on Intelligent Control (1999), and of the Conference Editorial Board for the IEEE Control Systems Society (1995–2000) and the Program Committee of the 39th IEEE Conference on Decision and Control (2000). Additionally, he was the Local Arrangements Chair for the 6th IEEE Conference on Control Applications (1997). Currently, he serves as the Associate Editor for IEEE TRANSACTIONS ON SIGNAL PROCESSING. He received the Michael J. Birck Fellowship from the University of Notre Dame (1990), the Harvey N. Davis Distinguished Teaching Award from Stevens Institute of Technology (1997), and the Faculty Early Career Development (CAREER) award from the National Science Foundation (1999). He is a member of Eta Kappa Nu.

Endre I. Sára (S'96) received the M.E. degree from the Technical University of Budapest, Budapest, Hungary, in 1996, and the Ph.D. degree from the Stevens Institute of Technology, Hoboken, NJ, in 1999, both in electrical engineering.

From 1993 to 1996, he was the Network Manager for the Technical University of Budapest. During 1996–1999, he was a Teaching Assistant for the Department of Electrical and Computer Engineering, Stevens Institute of Technology, Hoboken, NJ. Currently, he is a Network Engineer with Goldman Sachs & Co., New York. His current research interests include network management, network design, video traffic modeling, and performance analysis of ATM networks for video transmission.

Wei Sun (S'97) received the B.S. degree from Xidian University, Xi'an, China, in 1992, and the M.S. degree from the Chinese Academy of Telecommunications Technology (CATT), Beijing, China, in 1995, both in electrical engineering. He is currently working toward the Ph.D. degree in the Department of Electrical and Computer Engineering, Stevens Institute of Technology, Hoboken, NJ.

From 1993 to 1997, he was a Telecommunication Engineer with the R&D Center of Telecommunications Technology, CATT. Since August 1997, he has been a Research and Teaching Assistant with the Department of Electrical and Computer Engineering, Stevens Institute of Technology. His research interests include stochastic signal process, wireless communication, and broadband network traffic management.